Materials Research Express

PAPER • **OPEN ACCESS**

Multiple characterization of some glassy-alloys as photon and neutron shields: *In-silico* Monte Carlo investigation

To cite this article: U Perianolu *et al* 2021 *Mater. Res. Express* **8** 035202

Materials Research Express

PAPER

Multiple characterization of some glassy-alloys as photon and neutron shields: *In-silico* Monte Carlo investigation

U Perişanoğlu[1], F I El-Agawany[2], H O Tekin[3,4], E Kavaz[1], Hesham M H Zakaly[5,6,*], Shams A M Issa[5,7], M H M Zaid[8,*], H A A Sidek[8], K A Matori[8] and Y S Rammah[2]

[1] Physics Department, Faculty of Science, Ataturk University, Erzurum, Turkey
[2] Physics Department, Faculty of Science, Menoufia University, 32511 Shebin El-Koom, Menoufia, Egypt
[3] Medical Diagnostic Imaging Department, College of Health Sciences, University of Sharjah, Sharjah, United Arab Emirates
[4] Medical Radiation Research Center (USMERA), Uskudar University, 34672 Istanbul, Turkey
[5] Physics Department, Faculty of Science, Al-Azhar University, Assiut, 71524, Egypt
[6] Institute of Physics and Technology, Ural Federal University, Ekaterinburg 620000, Russia
[7] Physics Department, Faculty of Science, University of Tabuk, Tabuk, 71451, Saudi Arabia
[8] Department of Physics, University Putra Malaysia, 43400, Serdang, Selangor, Malaysia
[*] Authors to whom any correspondence should be addressed.

E-mail: khesham.mokhamed@urfu.ru, h.m.zakaly@gmail.com and mhmzaid@upm.edu.my

Keywords: glassy alloys, MCNPX, Shielding properties, Er20Tm20, Er20Tb20

OPEN ACCESS

RECEIVED
15 February 2021

REVISED
28 February 2021

ACCEPTED FOR PUBLICATION
2 March 2021

PUBLISHED
12 March 2021

Abstract

In the present work, the nuclear radiation shielding proficiency of eight glassy alloys (Gd25RE25-Co25Al25 (RE = Tb, Dy and Ho)) containing different amounts of rare earth elements was investigated with MCNPX simulation codes. Mass attenuation coefficients (μ/ρ) of the glassy alloys were simulated in the energy interval of 0.2–20 MeV by exploiting MCNPX codes, and the generated data were found to match with theoretical WinXCOM results. Next, other crucial photon attenuation parameters, effective atomic number (Z_{eff}), Half Value Layer (HVL), and Mean Free Path (MFP), were gotten out using μ/ρ values. It was seen that Er20Tm20 and Er20Tb20 samples replaced with Er by Gd had the highest Z_{eff} and μ/ρ values, whereas HVL and MFP values were the smallest among the other glassy alloys. Geometric progression (GP) procedure was enjoyed to achieve the exposure and energy absorption buildup factors (EBF and EABF) for the glassy alloys proposed. EABFs and EBFs took the largest and lowest values for Gd25Tb25 and Er20Tm20, respectively, to the other samples. Furthermore, the glassy alloys' neutron reduction abilities were estimated by acquiring fast neutron removal cross-sections ($\sum_R$). It was noticed that the $\sum_R$ values of the glassy alloys are increased with the rising sample density and seen to be comparable to $\sum_R$ values of water and ordinary concrete. The results obtained from this study are important in that they show that glassy alloys can be used as radiation shielding.

1. Introduction

In the last few years, ionizing radiation has more attractive applications in different fields such as medical area (radiotherapy, radiology, nuclear medicines), industry branch (test the void and insertion into the inner part of the material), and agricultural field (to differentiate between different types of woods, save the plants seeds and foods). On the other side, these radiations, especially γ-photons, can be travelled for a long kilometre and have high power to penetrate materials. This is because they have a very short wavelength (high energy). For the reasons mentioned above, radiations have harmful effects on the humans, environmental, and animals [1]. Several researchers and investigators have devoted significant efforts to finding more suitable radiation protection materials [2–8]. For example, in this literature, Kilic *et al* 2021 [9] studied the impact of Eu_2O_3 additive to zinc-borate on physical and nuclear radiation shielding properties of different types of samples, obtained in density and molar volume variations. The experimental analyses and simulation by MCNPX (version 2.6.0) showed that maximum nuclear shielding competence had been provided with maximum Eu_2O_3

Table 1. Sample code, density and weight fraction of each elements for the selected glassy alloys.

	Weight fraction of each element in the glassy alloys											
Sample code	**Al**	**Co**	**Ni**	**Y**	**Ag**	**Gd**	**Tb**	**Dy**	**Ho**	**Er**	**Tm**	Density g/cm^3
Gd25Tb25	0.067103	0.146567	—	—	—	0.391082	0.395248	—	—	—	—	**6.898**
Gd25Dy25	0.066512	0.145276	—	—	—	0.387635	—	0.400577	—	—	—	**6.9775**
Gd25Ho25	0.066116	0.144410	—	—	—	0.385327	—	—	0.404147	—	—	**7.04**
Er20Tb20	0.046957	0.102564	—	—	—	—	0.276584	0.282805	—	0.291089	—	**7.462**
Er20Tm20	0.046153	0.100808	—	—	—	—	—	0.277964	—	0.286106	0.288970	**7.68**
Gd20Ni20	0.047810	—	0.103996	—	—	0.278641	0.281609	0.287943	—	—	—	**7.47**
Gd20Co20	0.047790	0.104382	—	—	—	0.278521	0.281488	0.287819	—	—	—	**7.462**
RE10	0.023417	0.051146	0.050935	0.077159	0.093616	0.136473	0.137927	0.141029	0.143138	0.145160	—	**7.788**

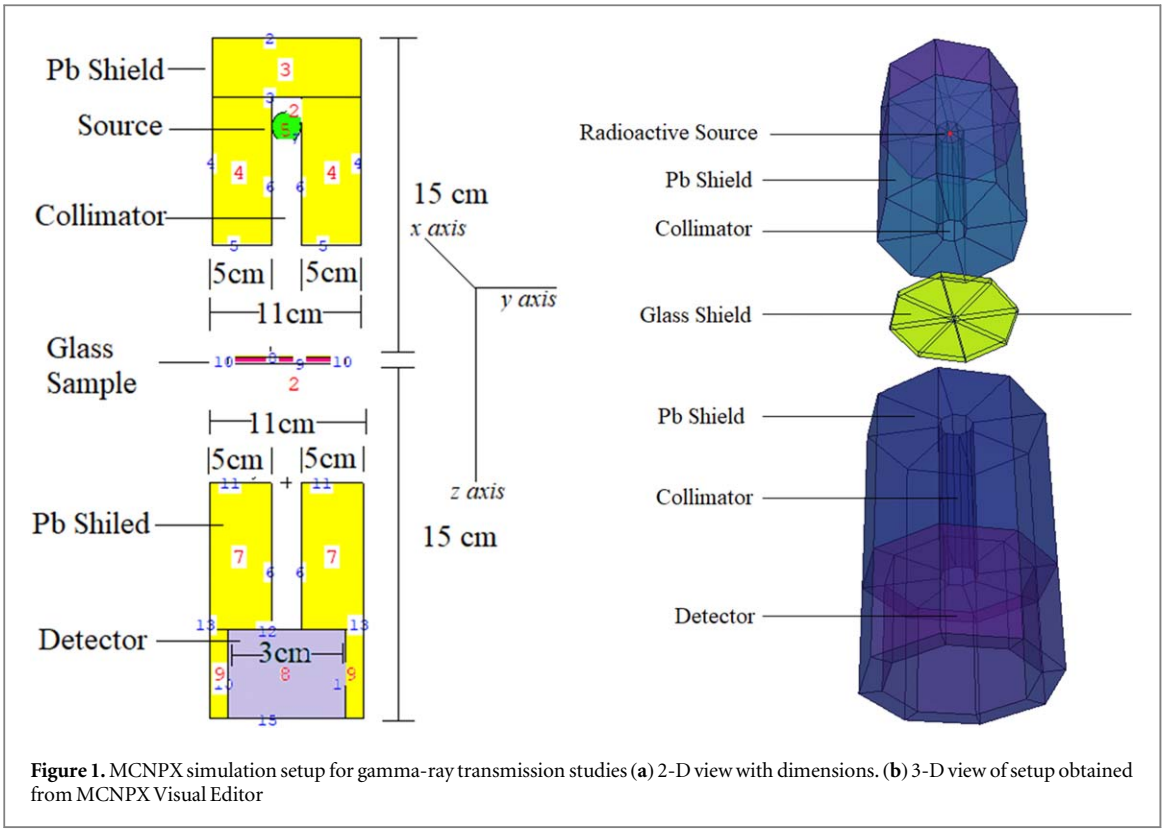

Figure 1. MCNPX simulation setup for gamma-ray transmission studies (**a**) 2-D view with dimensions. (**b**) 3-D view of setup obtained from MCNPX Visual Editor

concentration in the glass. The increasing Eu_2O_3 reinforcement has directly affected the glass behaviours against gamma-ray, fast neutrons and heavy charged particles such as alpha and proton [10]. Rammah *et al* [11] reported the influence of PbF_2 on properties of radiation shielding of nine different samples with the form of (100-X)TeO_2-XPbF_2: (where X = 10–90 mol%) glass-ceramics via the bond compression model and WinXcom software. The attenuation observed that increased by increasing the content of Pbf_2. The obtained results showed that the addition of Pb to the proposed samples improves their mechanical and radiation shielding properties. Many research studies have investigated which material or composition is better for blocking out ionizing radiation [12–17].

The shielding material must be planted between the radioactive source and the environment or workers to reduce or shun the harmful radiation exposure from the literature. Concretes, alloys, and polymers have been used widely as radiation shielding materials for their low-cost preparation and moulded in different sizes and shapes [18–24]. Nevertheless, these materials have many problems, such as crack formation for long time exposure to nuclear radiations, high opaque, and low in density [25]. Several investigators have been focused on using glass-ceramics and glasses as alternative radiation attenuation materials due to their high transparency in the visible region and can reduce radiations like photon and neutrons. Moreover, the optical, physical, mechanical, dielectric properties and shielding feature of glasses can be easily altered by choosing different additive materials such as heavy metal oxides and/or rare earths oxides [26–33]. Additionally, the production process of glass systems is easy, cheap, and can be produced in different sizes with high space homogeneity. Due to the heavy rare earth (RE = Tb, Gd, Tm, Dy, Ho, and others) based glassy alloys characterized by their exhibiting large magnetocaloric effect (MCE) and profuse magnetic structures, many researchers paid more efforts to develop new RE-based glassy alloys. Yu *et al* [34] have been studied the magneto-caloric effect (MCE) in amorphous $Gd_{50}Co_{50}$ alloy by minor addition of Zn in near room temperature. Yuan *et al*, [35] have been controlled in spin-glass (SG) behaviour and MCE in Gd-Ni-Al bulk metallic glasses. Li *et al* [36] have been studied the distinction of the SG behaviour and excellent MCE in $Er_{20}Dy_{20}Co_{20}Al_{20}RE_{20}$, where RE = Tb, Gd, and Tm) with high-entropy bulk metallic glasses. Xue *et al*, [37] reported the SG behaviour and MCE for $Gd_{25}RE_{25}Co_{25}Al_{25}$ (RE = Tb, Dy and Ho). Besides, a large number of RE-based glassy alloys showed ferromagnetic-paramagnetic transition and SG like behaviour, such as in [38, 39]. In the present work, the nuclear radiation security competences (parameters mentioned above) of selected RE-based glassy alloys from reference [37] have been evaluated. The nuclear radiation shielding parameters such as mass attenuation coefficient (μ/ρ), which is most essential parameter, linear attenuation coefficient (μ), half-value layer (HVL), mean free path (MFP), effective atomic number (Z_{eff}), buildup factors (EBF and EABF) and neutron removal cross-section were evaluated [40–49]. Considering the importance in literature for the scientific community, we

Table 2. Comparison between MAC values for eight glassy alloys using MCNP and XCOM software program at different photon energies.

	Gd25Tb25			Gd25Dy25			Gd25Ho25			Er20Tb20		
Photon energy (MeV)	**XCOM**	**MCNP**	**RD (%)**	**XCOM**	**MCNP**	**RD (%)**	**XCOM**	**MCNP**	**RD (%)**	**XCOM**	**MCNP**	**RD (%)**
0.02	38.130	39.254	−2.948	38.870	40.005	−2.919	39.780	40.547	−1.927	42.800	43.568	−1.795
0.06	9.358	9.683	−3.468	9.521	9.714	−2.023	9.738	9.752	−0.146	10.740	10.986	−2.293
0.08	4.412	4.451	−0.890	4.497	4.503	−0.140	4.595	4.609	−0.302	5.077	5.126	−0.973
0.1	2.451	2.473	−0.878	2.498	2.500	−0.100	2.554	2.563	−0.363	2.821	2.856	−1.253
0.356	0.154	0.157	−2.162	0.155	0.159	−2.277	0.157	0.160	−1.698	0.165	0.167	−0.956
0.511	0.100	0.102	−2.252	0.101	0.103	−2.181	0.102	0.104	−2.065	0.105	0.106	−1.324
0.662	0.080	0.080	−0.611	0.080	0.081	−1.663	0.080	0.086	−6.492	0.082	0.085	−4.156
1.17	0.054	0.055	−2.068	0.054	0.055	−2.533	0.054	0.057	−4.436	0.054	0.057	−4.658
1.25	0.052	0.052	−0.285	0.052	0.052	−0.167	0.052	0.054	−3.083	0.052	0.056	−6.401
1.33	0.050	0.051	−2.394	0.050	0.052	−2.907	0.050	0.052	−4.013	0.051	0.052	−3.752
5	0.037	0.037	−1.137	0.037	0.037	−1.340	0.037	0.039	−5.247	0.038	0.039	−3.224
8	0.039	0.039	−0.422	0.039	0.040	−1.599	0.039	0.040	−2.337	0.040	0.041	−1.628
10	0.041	0.041	−1.033	0.041	0.042	−1.995	0.041	0.042	−1.639	0.042	0.043	−0.529
15	0.045	0.045	−0.038	0.045	0.045	−0.060	0.046	0.046	−0.088	0.047	0.048	−2.180
20	0.049	0.049	−0.325	0.049	0.049	−0.436	0.049	0.051	−2.707	0.051	0.052	−2.031
Photon energy (MeV)	Er20Tm20			Gd20Ni20			Gd20Co20			RE10		
	XCOM	**MCNP**	**RD (%)**	**XCOM**	**MCNP**	**RD (%)**	**XCOM**	**MCNP**	**RD (%)**	**XCOM**	**MCNP**	**RD (%)**
0.02	45.270	45.985	−1.580	40.800	41.254	−1.113	40.370	41.126	−1.872	42.390	42.986	−1.405
0.06	11.290	11.313	−0.200	10.210	10.326	−1.132	10.190	10.287	−0.947	9.585	9.602	−0.182
0.08	5.345	5.366	−0.391	4.820	4.846	−0.546	4.810	4.827	−0.351	4.510	4.633	−2.722
0.1	2.973	2.995	−0.749	2.675	2.695	−0.756	2.669	2.686	−0.621	2.503	2.515	−0.466
0.356	0.171	0.174	−1.586	0.160	0.162	−1.210	0.160	0.161	−0.826	0.155	0.160	−3.225
0.511	0.107	0.110	−2.698	0.103	0.103	−0.735	0.102	0.103	−0.671	0.101	0.100	0.990
0.662	0.083	0.086	−2.920	0.081	0.083	−2.619	0.081	0.081	−0.686	0.080	0.081	−1.077
1.17	0.055	0.056	−2.682	0.054	0.055	−2.035	0.054	0.055	−1.897	0.054	0.055	−1.881
1.25	0.053	0.054	−1.940	0.052	0.053	−1.991	0.052	0.053	−1.393	0.052	0.053	−1.373
1.33	0.051	0.053	−3.704	0.050	0.052	−2.506	0.050	0.051	−2.225	0.050	0.051	−2.124
5	0.038	0.039	−2.897	0.038	0.038	−1.920	0.037	0.038	−1.881	0.037	0.038	−1.925
8	0.041	0.042	−2.367	0.040	0.040	−0.943	0.040	0.040	−0.586	0.040	0.040	−0.936
10	0.043	0.043	−1.021	0.042	0.042	−0.188	0.042	0.042	−0.474	0.041	0.042	−0.733
15	0.048	0.048	−0.405	0.047	0.047	−0.230	0.047	0.047	−0.474	0.046	0.047	−0.627
20	0.052	0.054	−2.873	0.051	0.051	−0.230	0.051	0.051	−0.464	0.050	0.050	−0.481

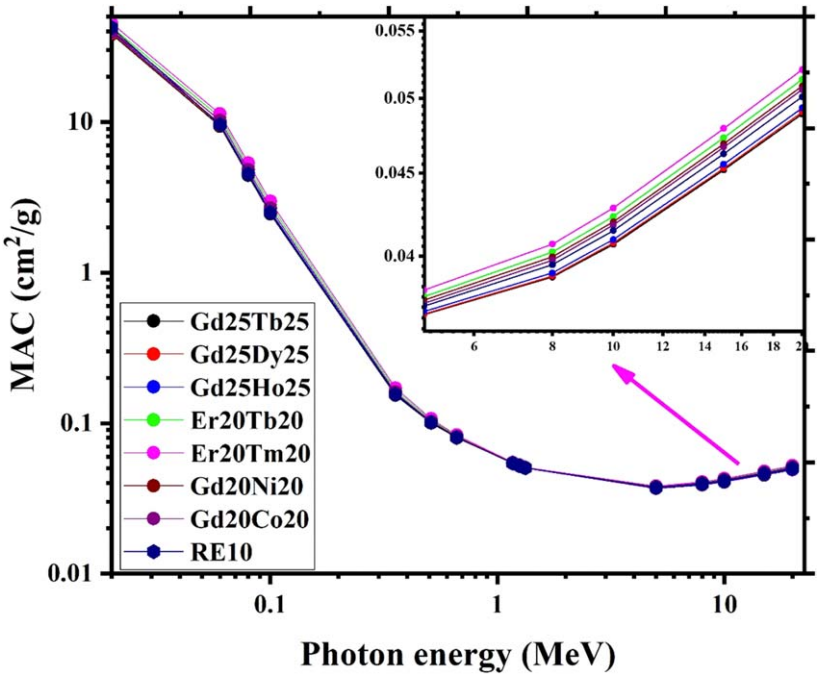

Figure 2. MAC for eight selected glassy alloys at different photon energy.

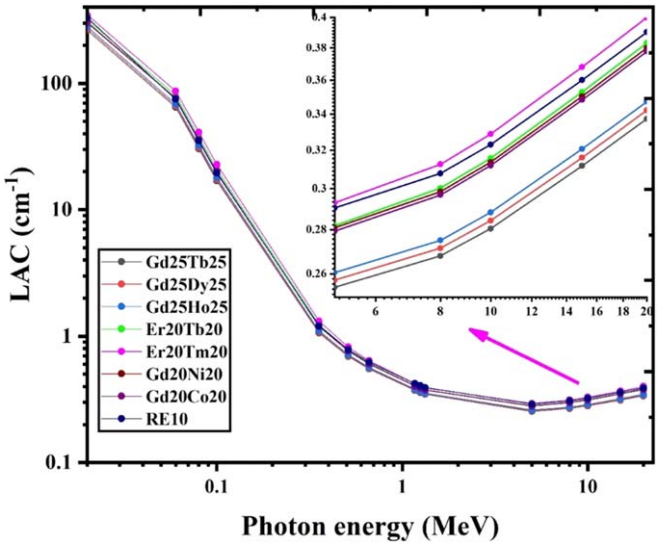

Figure 3. LAC for eight selected glassy alloys at different photon energy.

investigated the gamma shielding parameters of (Gd25RE25Co25Al25 (RE = Tb, Dy and Ho)) eight glassy alloys to demonstrate their usage as protective devices in many medical applications. Recent investigation outcomes would help a better understanding of rare earth elements impact on radiation shielding properties of glassy alloys.

2. Materials and methods

RE-based glassy alloys samples were chosen from reference [37]. Samples codes and weight fraction of each element and the corresponding density for the selected glassy alloys were listed in table 1.

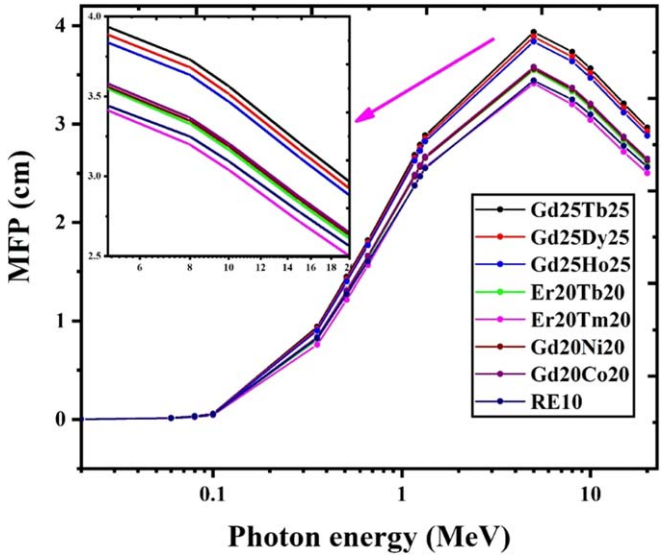

Figure 4. MFP for eight selected glassy alloys at different photon energy.

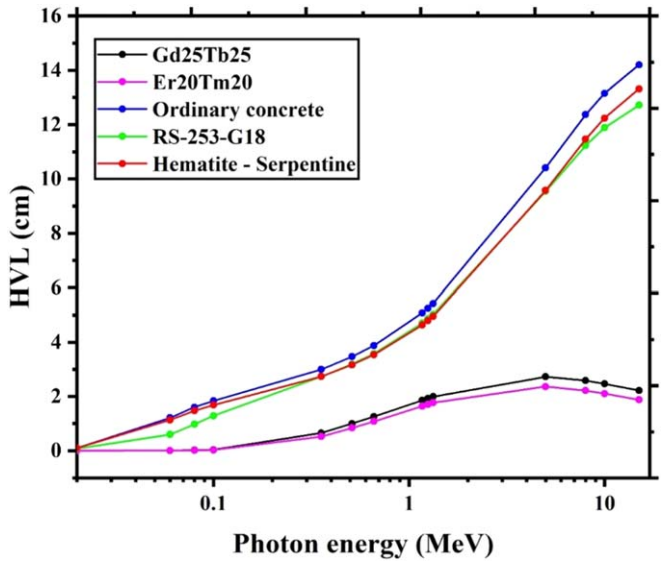

Figure 5. HVL for Gd25Tb25 and Er20Tm20 compared with different commercial material used as shielding materials at different photon energy.

2.1. Theory

The reduction of photons through the glassy alloys under investigation can be described Beer–Lambert rule [48, 49]:

$$I = I_o e^{-\mu x} \tag{1}$$

Where I and I_o refer to the photon numbers after passing the glassy alloys and initial incident photon numbers, respectively. Linear attenuation coefficient ((LAC, cm^{-1}) is denoted μ. The transmission factor for glassy alloys represented by the ratio I/I_o. The LAC is utilized to define the possibility of gamma-ray interaction with alloys per unit length. It can be theoretically obtained utilizing the mixture rule[40–49]:

$$\frac{\mu}{\rho} = \sum_i W_i \left(\frac{\mu}{\rho}\right)_i \tag{2}$$

where w_i refers to the weight fraction of the ith component in the glassy alloys, and $(\mu/\rho)_i$ stands the mass attenuation coefficient (MAC) of the ith component.

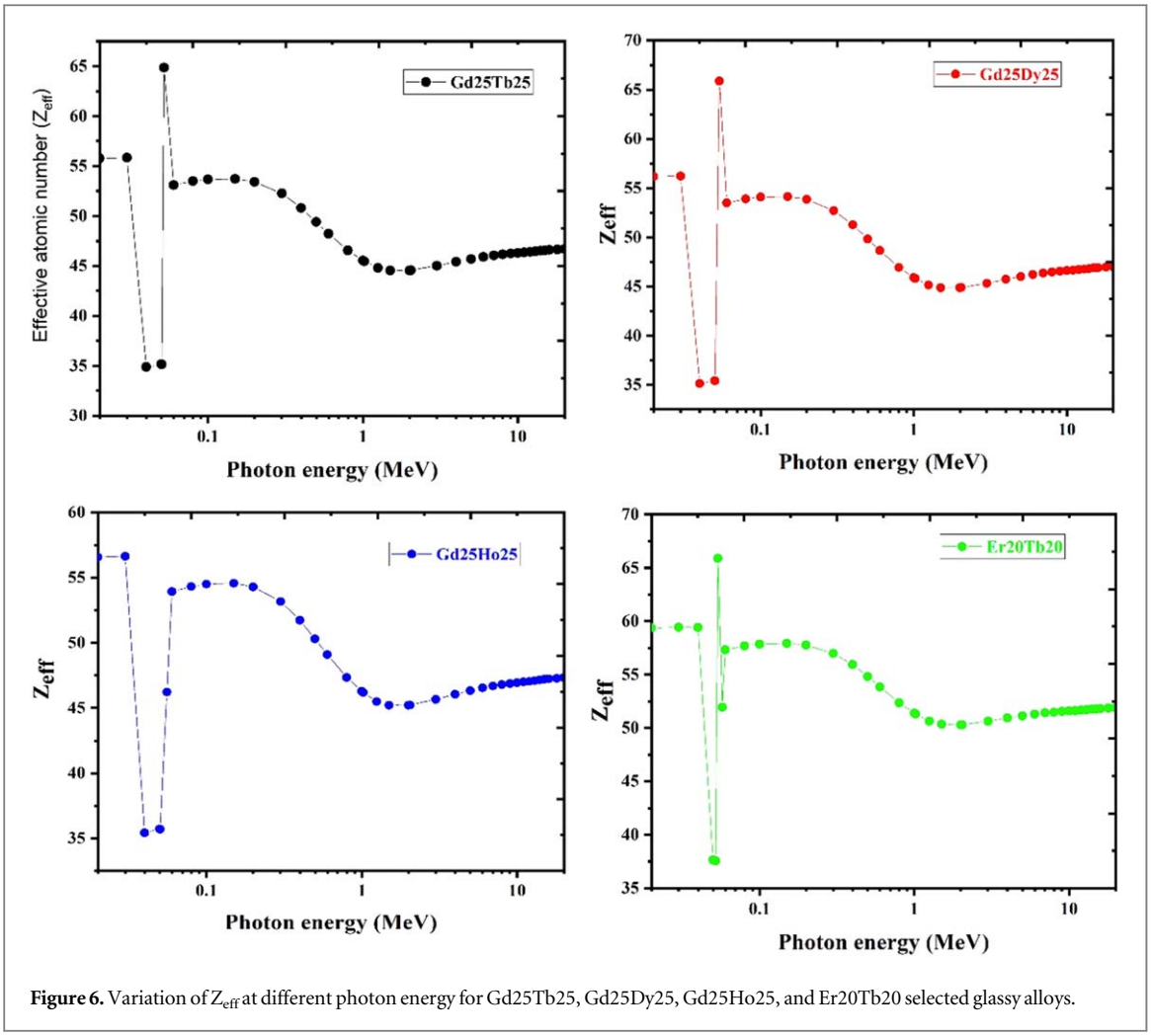

Figure 6. Variation of Z_{eff} at different photon energy for Gd25Tb25, Gd25Dy25, Gd25Ho25, and Er20Tb20 selected glassy alloys.

Grounded on both density and LAC of alloys, one get two effective shielding parameters named; mean free path (MFP) and half-value layer (HVL) can be found through the following equations [40–49].

$$HVL = \frac{\ln 2}{\mu} \text{ and } MFP = \frac{1}{\mu} \tag{3}$$

Furthermore, the effective atomic number (Z_{eff}) that define the multi-element alloys in its equivalent element, can be calculated through the following equation [48, 49].

$$Z_{eff} = \frac{\sum_i f_i A_i \left(\frac{\mu}{\rho}\right)_i}{\sum_j f_j \frac{A_j}{Z_j} \left(\frac{\mu}{\rho}\right)_j} \tag{4}$$

The causes of photon buildup in an environment are Compton scattering and multiple scattering events. The buildup factor is expressed by two different parameters: energy absorption and exposure buildup factor (EABF and EBF) [47]. For determining the buildup factors, geometric progression (GP) fitting coefficients were determined by interpolating equivalent atomic number (Z_{eq}) values[46]. Many works have reported detailed procedure of EABF and EBF calculations [44, 45].

For fast neutrons, Effective removal cross-sections (Σ_R) of the glassy alloys were figured out with the help of the formulas below[41]:

$$\sum_R / \rho = \sum_i W_i \left(\sum_R / \rho\right)_i \tag{5}$$

$$\sum_R = \sum_i \rho_i \left(\sum_R / \rho\right)_i \tag{6}$$

where $(\sum_R / \rho)_i$ refers to the mass removal cross-section of the ith constituent, and W_i and ρ denote the partial density (g/cm^3) and ith constituent's density, respectively.

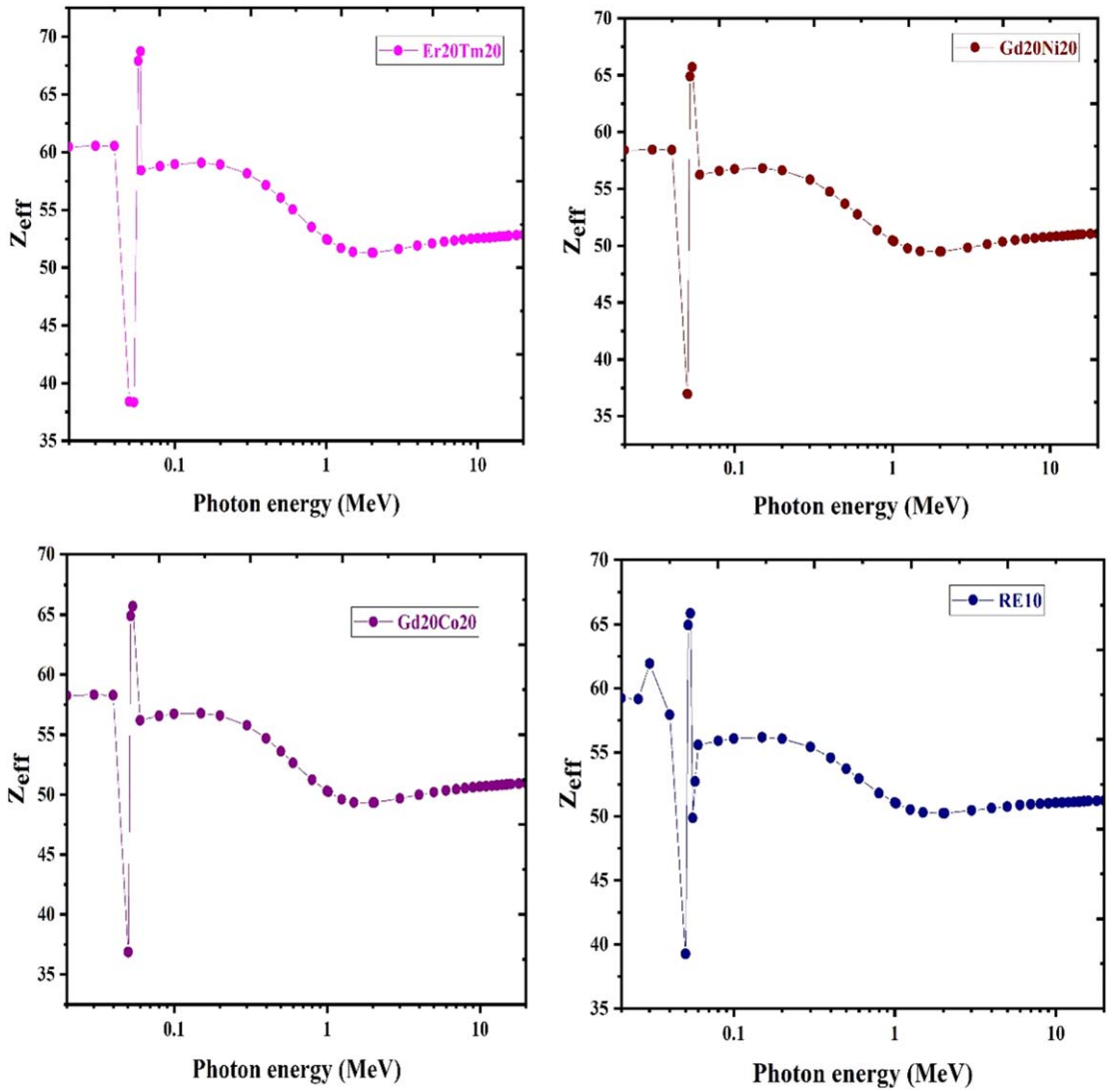

Figure 7. Variation of Z_{eff} at different photon energy for Er20Tm20, Gd20Ni20, Gd20Co20, and RE10 selected glassy alloys.

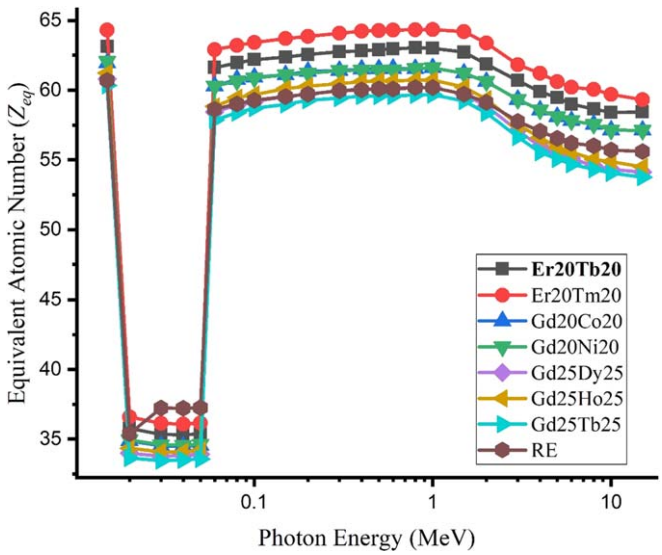

Figure 8. Equivalent atomic number (Z_{eq}) of the glassy alloys.

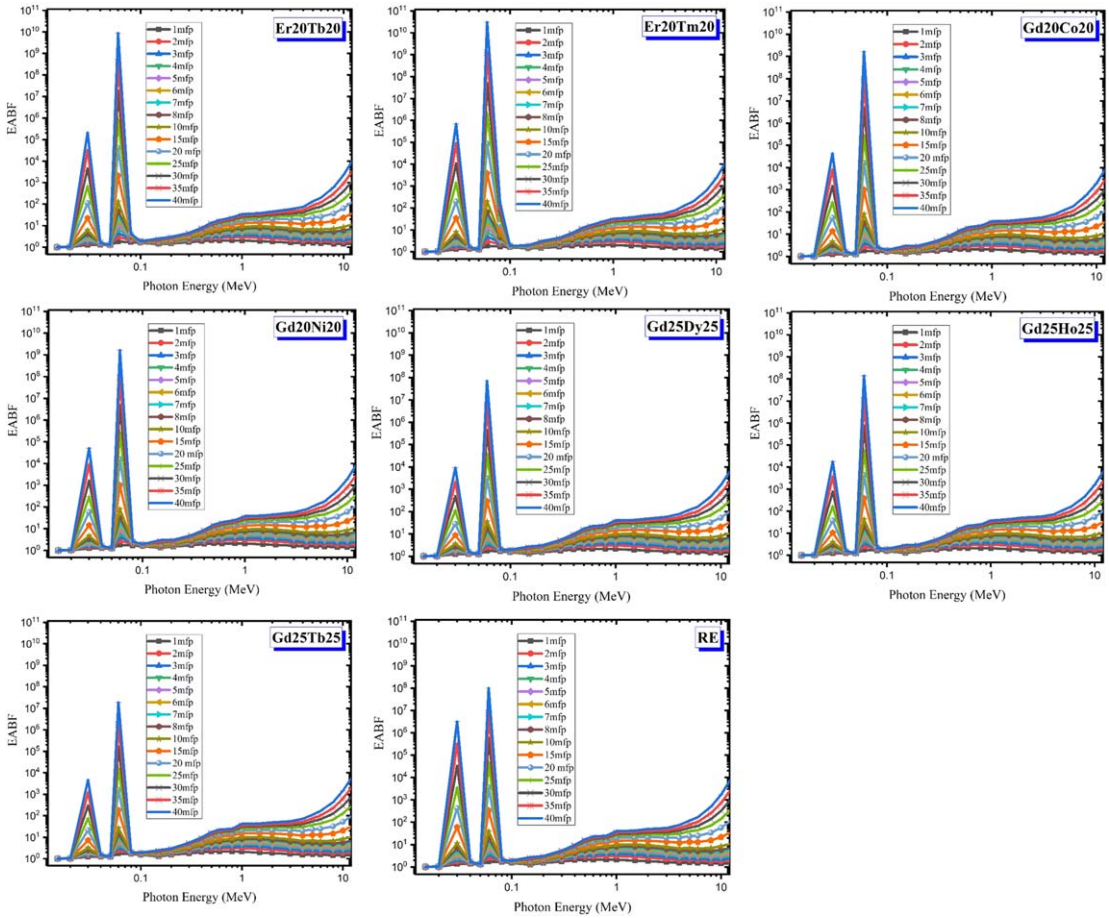

Figure 9. The EABF values of the glassy alloys against photon energy for different penetration depths.

2.2. MCNPX Simulation Procedure

The importance of numerical simulation techniques on nuclear radiation shielding studies is still hot topic in literature. During the numerical simulation, various types of outcomes can be obtained depending on the characteristics of the code that is being run. This section will discuss the technical properties of performed Monte Carlo simulations using the MCNPX code [16, 17, 50–55]. Reducing the radiation level to the safest levels is the most important criterion for a shield. Moreover, experimental conditions may not always be provided to conduct radiation studies. This is due to some specific reasons such as strict radiation studies regulations, biological risks of ionizing radiation and cost problems. Using numerical simulation methods is a well-known process for optimizing the shielding properties of materials before fabrication. In the present study, eight glassy alloys encoded Gd25Tb25, Gd25Dy25, Gd25Ho25, Er20Tb20, Er20Tm20, Gd20Ni20, Gd20Co20 and RE10 were created with their chemical features (See table 1). Primary, a specimen was modelled between point isotropic and F4 Tally Mesh detection fields as a cylindrical geometry. The cell environment of the specimen was filled with M1 definition, which was defined in the part of the material definition in the MCNPX input file. After, M1 was defined considering the elemental mass fraction of the glassy alloys. The Lambert-Beer law was employed to determine the mass attenuation coefficient at the range of 0.015–15 MeV. This process was repeated for each glass sample [56]. The view of the modelled simulation setup can be observed in figure 1. It is worth to be mention that visualization of modeling simulation setup was performed in Visual Editor of MCNP (VE X_22S).

3. Results and discussion

In this work, the simulation outcomes of μ/ρ values were initially achieved by employing MCNPX computer codes in the energy range 0.02–20 MeV. Next, for verifying the data generated with MCNPX codes, μ/ρ values of eight glassy alloys were derived using WinXCOM software. In table 2, the results found for μ/ρ are given with relative deviations between both methods. The relative deviation (RD%) between the two outcomes was calculated with the formula; $RD\% = ((\mu_{WinXCOM} - \mu_{MCNPX})/\mu_{WinXCOM})^{*}100$. The RD% varied in the range of

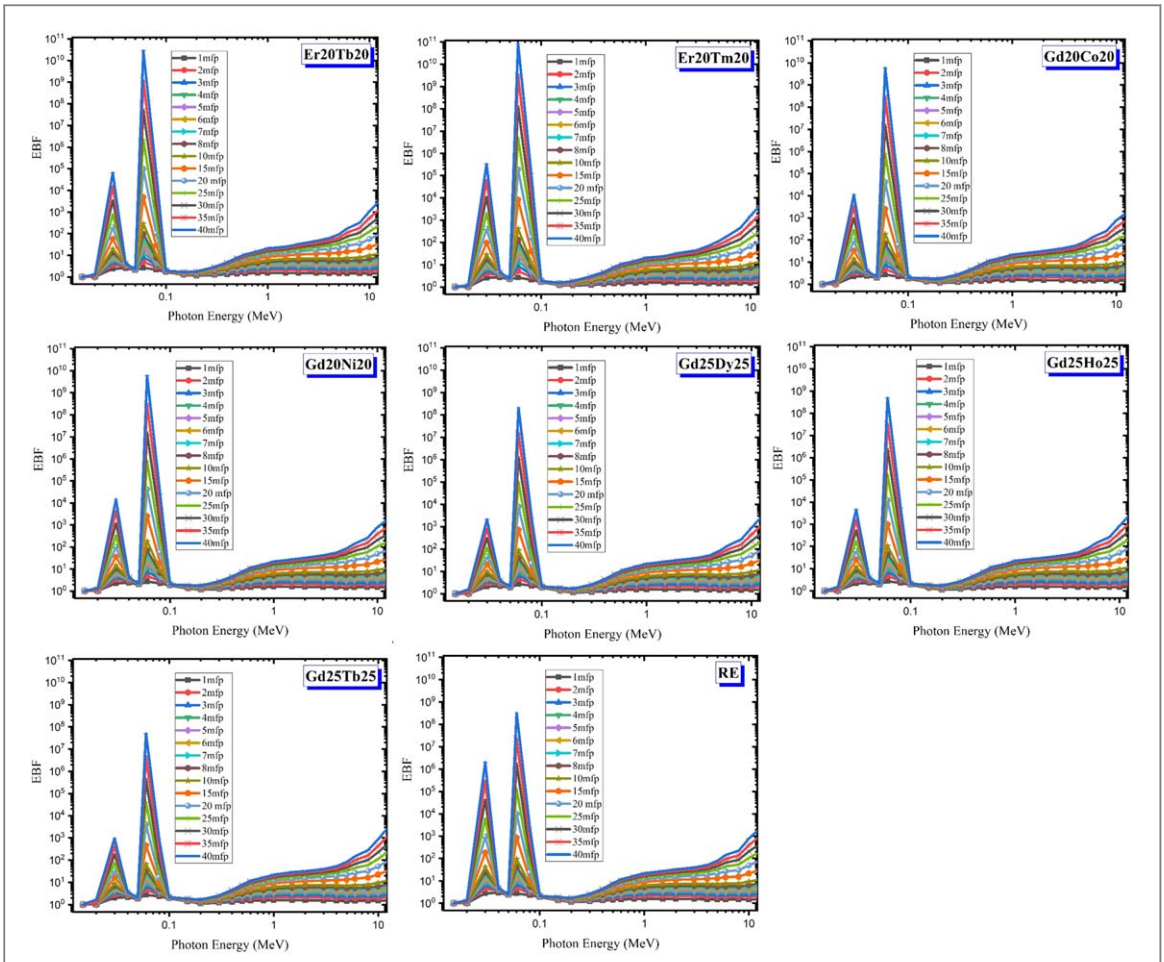

Figure 10. The EBF values of the glassy alloys against photon energy for different penetration depths.

−6.492–0.038. This shows that the μ/ρ values found by both methods support each other's. Also, figure 2 provides the change of μ/ρ values of glassy alloys for different photon energies. One can see from figure 2 that the μ/ρ values are declined as the energy level shifts to larger energies. The cross-section of the photoelectric effect changes with $Z^{4-5}/E^{3.5}$ at low energies, where photons interact maximum with the material. The μ/ρ of all glassy alloys possesses a strong addiction to the photon energy in this region. It is obvious from figure 2 that Er20Tm20 owns the largest μ/ρ values among the other glassy alloys. At 0.1–4 MeV energy range, the Compton scattering process starts to prevail with the boosting energy, and the dependence of μ/ρ values on photon energy impoverishes (1/E). As can be noticed from figure 2, μ/ρ values of glassy alloys enhance slowly with rising photon energy after 5 MeV since pair production whose cross-section is associated with Z^2 grows into a predominant mechanism at high energy levels. In all energies, Er20Tm20 alloy got the highest μ/ρ values. Figure 3 visualizes the trend of Linear Attenuation Coefficient (LAC) values against photon energy. The differences in LAC values, which have a curve similar to the μ/ρ values, have become more evident with the density of the samples. Just like the μ/ρ values, the Er20Tm20 sample has the largest LAC values. The changes of MFP and HVL values of glassy alloys against photon energy are presented by figures 4 and 5, respectively. MFP and HVL are easily found, providing knowledge about the penetration of photons into the shield material. It is obvious that MFPs of all glassy alloys are stationary nearly versus photon energy up to 0.1 MeV. Between 0.1–4 MeV, the MFPs tend to increase speedily, and the MFP curves become distinct in this region. Er20Tm20 owns the smallest MFP values, while the lowest MFP values belong to Gd25Tb25. In figure 4, it is evident that MFP values gradually decrease as the photon energy rises after 5 MeV. Since the cross-sections of photoelectric absorption and pair production change with Z^{4-5} and Z^2, photons lose more energy in these processes, and most of them annihilated. Therefore, smaller material thickness is sufficient in the related energies compared to medium energies. Secondary and Compton scatterings in medium energies cause larger MFP values. It is seen that Gd25Tb25 and Er20Tm20 samples, which have the smallest and largest HVL values among the glassy alloys selected in figure 5, compare with some traditional shield materials. It is noteworthy that the proposed glassy alloys have almost six times smaller HVL values than the previously reported ordinary concrete, hematite-serpentine concrete, and RS-253-G18 glass samples. The photon energy dependency of effective atomic

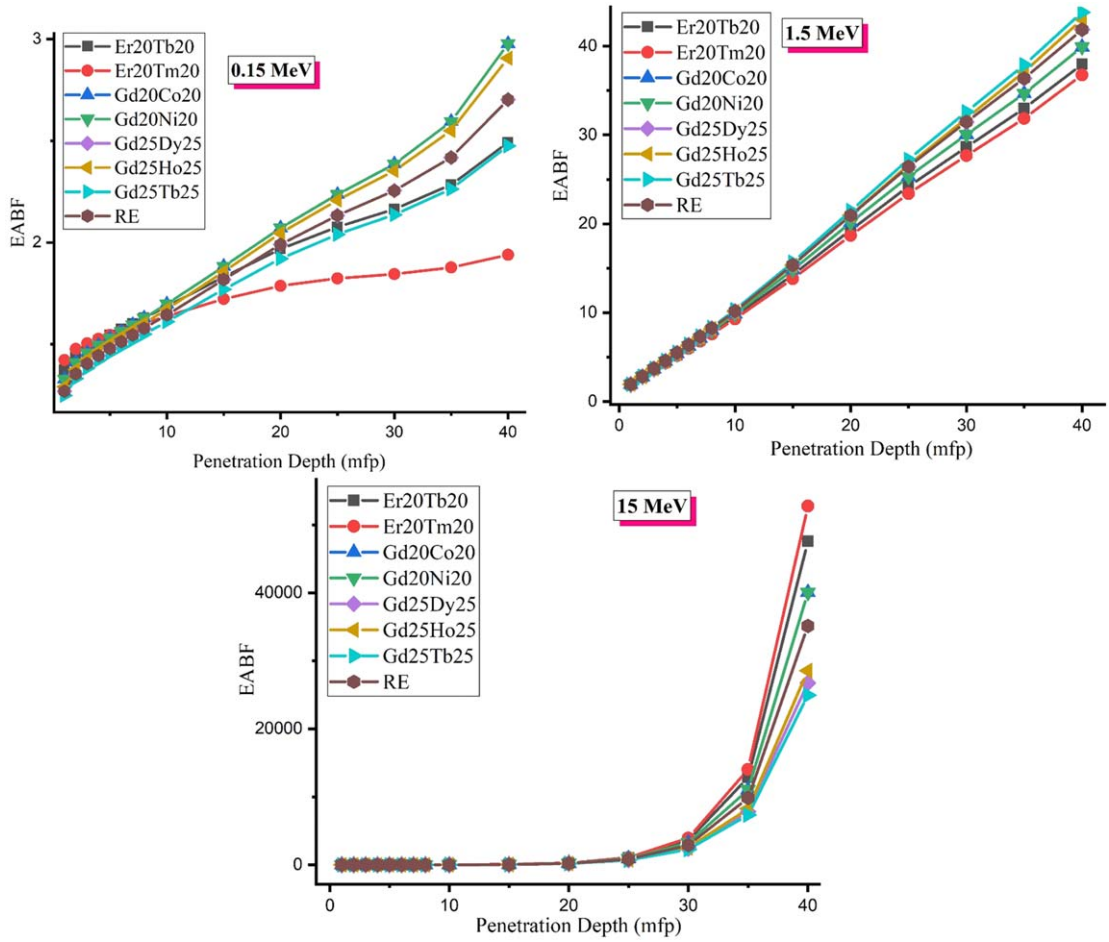

Figure 11. The EABF values of glassy alloys versus the penetration depths at 0.15, 1.5 and 15 MeV.

numbers (Z_{eff}) of the glassy alloys are indicated in figures 6 and 7. The behaviour of Z_{eff} values by photon energy is based on the main photon interactions. Depending on the elemental composition of glassy alloys, sudden and large jumps are observed at around 0.05 MeV. The source of these sudden peaks are the K X-ray absorption edge of the elements Gd, Tb, Dy, Ho, Er and Tm (50.23, 51.99, 53.78, 55.61, 57.48. and 59.38 keV, respectively). The change of Z_{eff} values in medium energies is slow due to the Compton scattering process. It is light that the Er20Tm20 and Er20Tb20 glassy alloys with high Er content have the highest values of Z_{eff}. After 1 MeV, Z_{eff} values start to increase again due to the Pair production process. Figure 8 depicts the fluctuations of the Z_{eq} values with gamma-ray energy. It can be understood from figure 8 that as the ratio of high atomic number lanthanides in the glassy alloys is increased, Z_{eq} values are raised. Z_{eq} values displayed abrupt jumps in the absorption edges of lanthanides found in the contents of the samples studied around 0.5 MeV. EBFs and EABFs of glassy alloys are acquired employing GP fitting coefficients at 0.15–15 MeV photon energies, and table 3 depicts the b, a, c, Xk, d parameters and Z_{eq} values for Er20Tm20 sample as an illustration. Figures 9 and 10 exhibit the variety of EABF and EBF of the glassy alloys versus photon energy at various penetration depths. The curves of EBF and EABF for the glassy alloys change with photon energy similarly. The glassy alloys interact with low and high-energy photons in photoelectric absorption (PA) and pair production (PP) mechanisms respectively. Since the cross-section of PA with the material depends on Z^{4-5}, the dramatic increments are observed in the low energy levels, the absorption edges of lanthanides. It is remarkable that as the amount of related lanthanide in the glassy alloy grows, the intensity of these peaks enhances. The rising in the number of secondary scatterings at the Compton process causes the increments of EABF and EBF values for the glassy alloys after 0.1 MeV. Next, the EABFs and EBFs for the glassy alloys are raised again at high energy levels where PP is the main process. The EABF and EBF values are highest especially for glassy alloys which have larger Z_{eq} values since the PP cross-section changes with Z^2. It is clear from figures 9 and 10 that the EABFs are larger than the EBFs for all of glassy alloys. This means that the buildup of the photons in the material is higher than in the air. While the Er20Tm20 and Er20Tb20 samples have the lowest buildup factors, the largest values of EABF and EBF belong to Gd25Tb25. Figures 11 and 12 indicate the variation of both buildup factors depending on the penetration depth for three different selected energies. The buildup factors enhance against penetration depth at 0.015 MeV. With

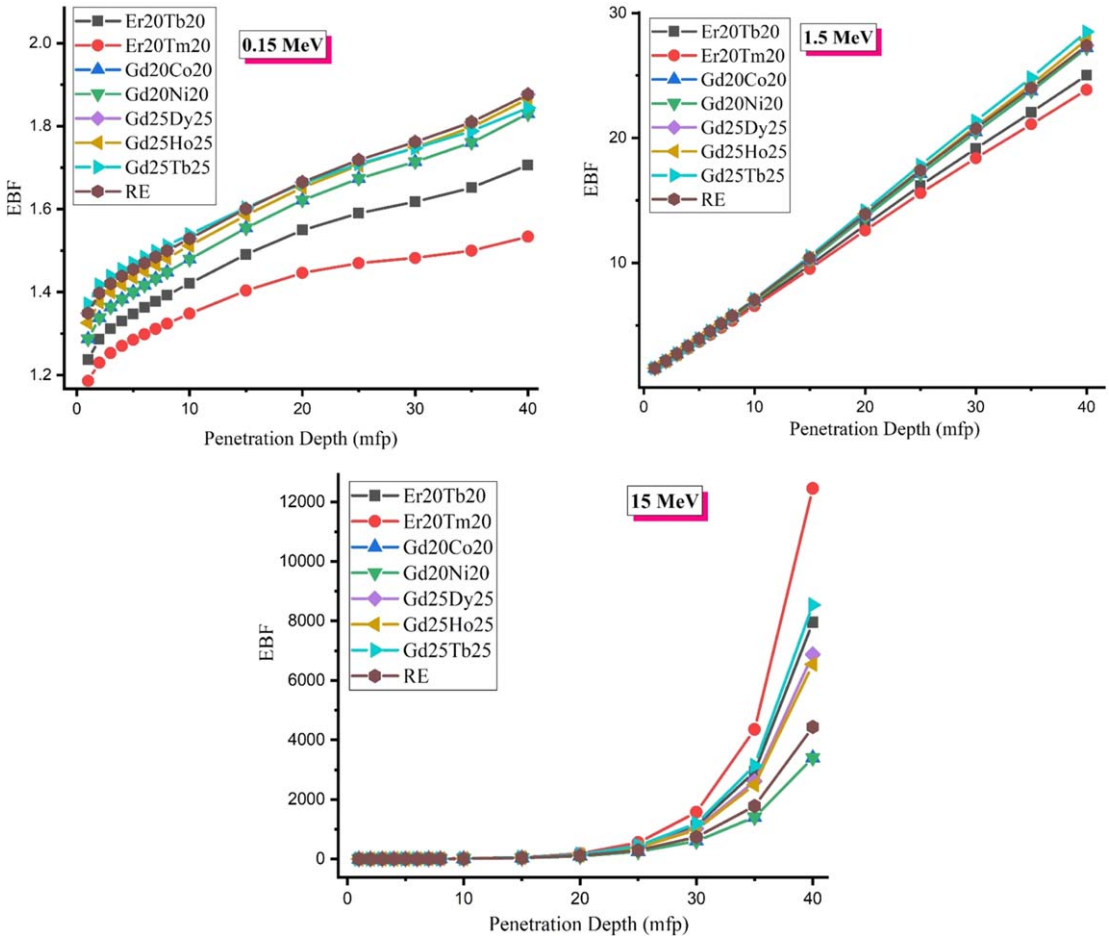

Figure 12. The EABF values of glassy alloys versus the penetration depths at 0.15, 1.5 and 15 MeV.

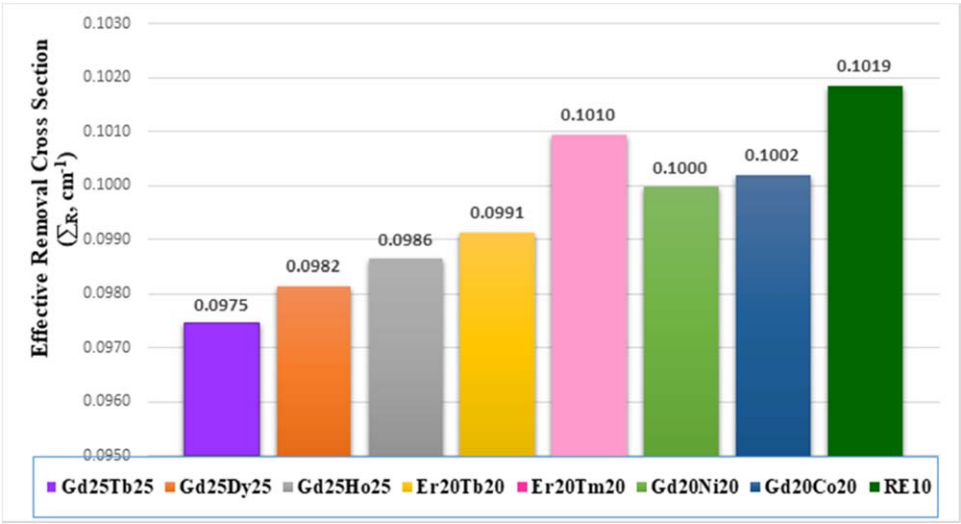

Figure 13. Fast neutron removal cross section values of the glassy alloys.

the enhancing penetration depth, the curves of EABF and EBF begin to diverge depending on the elemental content of the glassy alloys. The glassy alloys containing Er receive significantly smaller EABF and EBF values for all penetration depths. At 1.5 MeV, the increment of the EABF and EBFs linearly with raising penetration depth proves the change of Compton scattering cross-section with Z. For 15 MeV, the variation of buildup factors with the depth of penetration is completely opposite to the other two energies. In this energy, Gd25Tb25 sample has the lowest and Er20Tm20 sample has the largest EABF and EBF values. This is because at high energies, the

Table 3. Equivalent atomic numbers, G-P Fitting Parameters for EBF and EABF respectively for Er20Tm20 glassy alloy.

		G-P Fitting Parameters for EBF					*G-P Fitting Parameters for EABF*				
Energy (MeV)	Z_{eq}	**a**	**b**	**c**	**d**	X_k	**a**	**b**	**c**	**d**	X_k
1.50E-02	64.310	1.001	0.660	0.078	23.140	0.006	1.001	0.612	0.107	12.090	−0.037
2.00E-02	36.590	1.010	0.274	0.441	13.020	−0.488	1.009	0.315	0.328	13.680	−0.290
3.00E-02	36.130	2.565	0.793	0.149	26.410	−0.204	1.310	0.810	0.161	21.740	−0.141
4.00E-02	36.070	2.691	0.339	0.128	23.790	−0.094	1.302	0.367	0.119	27.910	−0.158
5.00E-02	36.140	2.207	0.166	−0.036	15.050	−0.028	1.255	0.175	0.045	11.140	0.006
6.00E-02	62.900	2.671	1.349	0.092	18.620	−0.087	1.872	1.316	0.098	18.070	−0.105
8.00E-02	63.210	2.100	0.587	0.242	16.950	−0.203	1.725	0.567	0.204	15.950	−0.174
1.00E-01	63.410	1.639	0.244	−0.014	19.350	0.062	1.632	0.226	0.046	18.950	0.040
1.50E-01	63.700	1.186	0.176	0.437	13.170	−0.260	1.422	0.087	0.614	13.300	−0.326
2.00E-01	63.850	1.159	0.392	0.230	14.040	−0.124	1.489	0.169	0.477	13.910	−0.259
3.00E-01	64.080	1.234	0.575	0.136	14.590	−0.078	1.663	0.302	0.317	13.990	−0.205
4.00E-01	64.230	1.326	0.657	0.104	13.970	−0.057	1.878	0.406	0.243	13.700	−0.158
5.00E-01	64.270	1.396	0.747	0.076	14.070	−0.045	2.016	0.513	0.187	13.770	−0.129
6.00E-01	64.320	1.446	0.804	0.059	13.750	−0.038	1.968	0.622	0.135	13.800	−0.095
8.00E-01	64.330	1.503	0.872	0.038	13.710	−0.027	2.049	0.705	0.102	13.640	−0.070
1.00E + 00	64.340	1.530	0.932	0.023	13.530	−0.022	2.019	0.786	0.075	14.510	−0.063
1.50E + 00	64.200	1.523	1.008	0.002	13.010	−0.012	1.898	0.910	0.034	13.360	−0.036
2.00E + 00	63.380	1.503	1.019	0.006	12.980	−0.022	1.797	0.893	0.048	13.340	−0.058
3.00E + 00	61.830	1.471	1.042	0.006	13.210	−0.031	1.632	0.876	0.064	13.410	−0.086
4.00E + 00	61.220	1.426	1.042	0.015	13.300	−0.045	1.499	0.861	0.078	13.670	−0.103
5.00E + 00	60.610	1.435	0.995	0.036	13.600	−0.065	1.596	0.752	0.127	14.060	−0.151
6.00E + 00	60.200	1.455	0.958	0.053	13.870	−0.079	1.501	0.807	0.108	14.190	−0.127
8.00E + 00	60.050	1.463	0.964	0.059	14.000	−0.084	1.432	0.877	0.092	14.440	−0.110
1.00E + 01	59.690	1.482	1.014	0.054	14.040	−0.080	1.426	0.927	0.088	14.160	−0.112
1.50E + 01	59.320	1.526	1.129	0.038	13.880	−0.068	1.405	1.104	0.061	13.970	−0.094

probability of photons interacting with material atoms is proportional to Z^2, so secondary scatterings are more in samples with large Z_{eq}. Finally, the resistance of the proposed glassy alloys to fast neutron radiation was investigated. For this purpose, the fast neutron removal cross sections ($\sum_R$) of the samples were gotten and illustrated in figure 13. The $\sum_R$ values for all glassy alloys are really near each other and comparable to good neutron shields such as water ($\sum_R$: 0.1030 cm^{-1}) and ordinary concrete ($\sum_R$: 0.0945 cm^{-1}). The high densities of Er20Tm20 and RE samples ensure that $\sum_R$ values are highest among the others. These results reveal that glassy alloys can be alternative shield materials for gamma energies which are important for applications of ionizing radiation and neutron radiation.

4. Conclusion

In this study, the usability of eight glassy alloys with different compositions and with high amounts of Gd, Tb, Dy, Ho, Er and Tm lanthanides as nuclear radiation shields was evaluated. Firstly, the mass attenuation coefficients (μ/ρ) of glassy alloys were produced with MCNPX simulation codes, and the outcomes of the simulation were compared with the theoretical WinXCOM values to ensure their accuracy. Next, the gamma protection parameters, LAC, MFP, HVL and $Z_{eff,}$ calculated employing μ/ρ values, were acquired in the energy range 0.02–20 MeV. LAC of the studied glassy alloys follows the trend: Er20Tm20 > RE10 > Er20Tb20 > Gd20Ni20 > Gd20Co20 > Gd25Ho25 > Gd25Dy25 > Gd25Tb25, while HVL follows the trend: Er20Tm20 < RE10 < Er20Tb20 < Gd20Ni20 < Gd20Co20 < Gd25Ho25 < Gd25Dy25 < Gd25Tb25. Z_{eff} follows the trend Er20Tm20 > RE10 > Er20Tb20 > Gd20Ni20 > Gd20Co20 > Gd25Ho25 > Gd25Dy25 > Gd25Tb25. Er20Tm20 and Er20Tb20 samples containing Er owned the largest MAC and Z_{eff} values, while they took much smaller HVL and MFP values than traditional shield materials and all glassy alloys studied. GP fitting method was operated to obtain the energy absorption and exposure buildup factors (EABF and EBF) of the glassy alloys for photon energies of 0.15 MeV to 15 MeV. The computations expose that the minimum EABFs and EBFs were gotten for the Er20Tm20 sample. Besides, the removal cross-section of fast neutron (ΣR) for the proposed glassy alloys were determined. It was deduced that the glassy alloys with higher specific gravity possess the largest Σ_R values and the Er20Tm20 and RE samples had the nearly same skill of neutron retention as water and conventional concrete.

Data availability statement

No new data were created or analysed in this study.

ORCID iDs

H O Tekin https://orcid.org/0000-0002-0997-3488
E Kavaz https://orcid.org/0000-0002-7016-2510
Hesham M H Zakaly https://orcid.org/0000-0002-7645-9964
Shams A M Issa https://orcid.org/0000-0002-9166-7497
M H M Zaid https://orcid.org/0000-0001-6734-800X
Y S Rammah https://orcid.org/0000-0003-3106-5571

References

[1] Beir V 1996 Health Effects of Exposure to Low Levels of Ionizing Radiation: BEIR V - National Research Council, Division on Earth and Life Studies, Commission on Life Sciences, Committee on the Biological Effects of Ionizing Radiation (BEIR V) - Google Book
[2] Sayyed M I 2016 Investigation of shielding parameters for smart polymers *Chinese J. Phys.* **54** 408–15
[3] Rammah Y S, Abouhaswa A S, Sayyed M I, Tekin H O and El-Mallawany R 2019 Structural, UV and shielding properties of ZBPC glasses *J. Non. Cryst. Solids* **509** 99–105
[4] Abouhaswa A S, Rammah Y S, Sayyed M I and Tekin H O 2019 Synthesis, structure, optical and gamma radiation shielding properties of B_2O_3-PbO_2-Bi_2O_3 glasses *Compos. Part B Eng.* **172** 218–25
[5] Zakaly H M H, Saudi H A, Issa S A M, Rashad M, Elazaka A I, Tekin H O and Saddeek Y B 2020 Alteration of optical, structural, mechanical durability and nuclear radiation attenuation properties of barium borosilicate glasses through BaO reinforcement: experimental and numerical analyses *Ceram. Int* **47** 5587–96
[6] Elazaka A I, Zakaly H M H, Issa S A M, Rashad M, Tekin H O, Saudi H A, Gillette V H, Erguzel T T and Mostafa A G 2021 New approach to removal of hazardous Bypass Cement Dust (BCD) from the environment: 20Na2O-20BaCl2-(60-x)B_2O_3-(x)BCD glass system and Optical, mechanical, structural and nuclear radiation shielding competences *J. Hazard. Mater.* **403** 123738
[7] El-Mallawany R, Sayyed M I, Dong M G and Rammah Y S 2018 Simulation of radiation shielding properties of glasses contain PbO *Radiat. Phys. Chem.* **151** 239–52
[8] Sayyed M I and Lakshminarayana G 2018 Structural, thermal, optical features and shielding parameters investigations of optical glasses for gamma radiation shielding and defense applications *J. Non. Cryst. Solids* **487** 53–9
[9] Kilic G, Issa S A M, Ilik E, Kilicoglu O and Tekin H O 2021 A journey for exploration of Eu_2O_3 reinforcement effect on zinc-borate glasses: synthesis, optical, physical and nuclear radiation shielding properties *Ceram. Int.* **47** 2572–83
[10] Saudi H A, Abd-Allah W M and Shaaban K S 2020 Investigation of gamma and neutron shielding parameters for borosilicate glasses doped europium oxide for the immobilization of radioactive waste *J. Mater. Sci., Mater. Electron.* **31** 6963–76
[11] Rammah Y S, Olarinoye I O, El-Agawany F I, El-Adawy A and Yousef E S 2021 The impact of PbF2 on the ionizing radiation shielding competence and mechanical properties of TeO_2–PbF2 glasses and glass-ceramics *Ceram. Int.* **47** 2547–56
[12] Tekin H O, Kassab L R P, Issa S A M, Dias da Silva Bordon C, Al-Buriahi M S, de Oliviera Pereira Delboni F, Kilic G and Magalhaes E S 2020 Structural and physical characterization study on synthesized tellurite (TeO2) and germanate (GeO_2) glass shields using XRD, Raman spectroscopy, FLUKA and PHITS *Opt. Mater. (Amst).* **110**
[13] Zakaly H M H, Rashad M, Tekin H O, Saudi H A, Issa S A M and Henaish A M A 2021 Synthesis, optical, structural and physical properties of newly developed dolomite reinforced borate glasses for nuclear radiation shielding utilizations: an experimental and simulation study *Opt. Mater. (Amst).* **114** 110942
[14] Issa S A M, Rashad M, Zakaly H M H, Tekin H O and Abouhaswa A S 2020 Nb_2O_5-Li_2O-Bi_2O_3-B_2O_3 novel glassy system: evaluation of optical, mechanical, and gamma shielding parameters *J. Mater. Sci., Mater. Electron.* (https://doi.org/10.1007/s10854-020-04707-7)
[15] Ali A M *et al* 2020 Promising applicable heterometallic Al_2O_3/PbO_2 nanoparticles in shielding properties *J. Mater. Res. Technol.* **9** 13956–62
[16] Tekin H O, Kassab L R P, Kilicoglu O, Magalhães E S, Issa S A M and da Silva Mattos G R 2020 Newly developed tellurium oxide glasses for nuclear shielding applications: An extended investigation *J. Non. Cryst. Solids* **528** 119763
[17] Tekin H O, Issa S A M, Kavaz E and Altunsoy Guclu E E 2019 The direct effect of Er_2O_3 on bismuth barium telluro borate glasses for nuclear security applications *Mater. Res. Express* **6** 115212
[18] Issa S A M, Zakaly H M H, Pyshkina M, Mostafa M Y A, Rashad M and Soliman T S 2021 Structure, optical, and radiation shielding properties of PVA–$BaTiO_3$ nanocomposite films: An experimental investigation *Radiat. Phys. Chem.* **180** 109281
[19] Kavaz E 2019 An experimental study on gamma ray shielding features of lithium borate glasses doped with dolomite, hematite and goethite minerals *Radiat. Phys. Chem.* **160** 112–23
[20] Singh J, Singh H, Sharma J, Singh T and Singh P S 2018 Fusible alloys: a potential candidate for gamma rays shield design *Prog. Nucl. Energy* **106** 387–95
[21] Singh V P, Shirmardi S P, Medhat M E and Badiger N M 2015 Determination of mass attenuation coefficient for some polymers using Monte Carlo simulation *Vacuum* **119** 284–8
[22] Olukotun S F, Gbenu S T, Ibitoye F I, Oladejo O F, Shittu H O, Fasasi M K and Balogun F A 2018 Investigation of gamma radiation shielding capability of two clay materials *Nucl. Eng. Technol.* **50** 957–62
[23] Henaish A M A, Mostafa M, Salem B I, Zakaly H M H, Issa S A M, Weinstein I A and Hemeda O M 2020 Spectral, electrical, magnetic and radiation shielding studies of Mg-doped Ni–Cu–Zn nanoferrites *J. Mater. Sci., Mater. Electron.* **31** 20210–22
[24] Sharma A, Sayyed M I, Agar O, Kaçal M R, Polat H and Akman F 2020 Photon-shielding performance of bismuth oxychloride-filled polyester concretes *Mater. Chem. Phys.* **241** 122330
[25] Kaur S and Singh K J 2014 Investigation of lead borate glasses doped with aluminium oxide as gamma ray shielding materials *Ann. Nucl. Energy* **63** 350–4

[26] Al-Buriahi M S and Rammah Y S 2019 Investigation of the physical properties and gamma-ray shielding capability of borate glasses containing PbO, Al_2O_3 and Na_2O *Appl. Phys. A Mater. Sci. Process.* **125** 717
[27] Al-Hadeethi Y, Sayyed M I and Rammah Y S 2019 Investigations of the physical, structural, optical and gamma-rays shielding features of B2O3—Bi2O3—ZnO—CaO glasses *Ceram. Int.* **45** 20724–32
[28] Rammah Y S, Sayyed M I, Ali A A, Tekin H O and El-Mallawany R 2018 Optical properties and gamma-shielding features of bismuth borate glasses *Appl. Phys. A* **124** 832
[29] Rammah Y S, Askin A, Abouhaswa A S, El-Agawany F I and Sayyed M I 2019 Synthesis, physical, structural and shielding properties of newly developed B_2O_3–ZnO–PbO–Fe_2O_3 glasses using Geant4 code and WinXCOM program *Appl. Phys. A Mater. Sci. Process.* **125** 523
[30] Sayyed M I, El-Mesady I A, Abouhaswa A S, Askin A and Rammah Y S 2019 Comprehensive study on the structural, optical, physical and gamma photon shielding features of B_2O_3-Bi_2O_3-PbO-TiO_2 glasses using WinXCOM and Geant4 code *J. Mol. Struct.* **1197** 656–65
[31] Sayyed M I, Rammah Y S, Abouhaswa A S, Tekin H O and Elbashir B O 2018 ZnO-B_2O_3-PbO glasses: Synthesis and radiation shielding characterization *Phys. B Condens. Matter* **548** 20–6
[32] Issa S A M, Tekin H O, Elsaman R, Kilicoglu O, Saddeek Y B and Sayyed M I 2019 Radiation shielding and mechanical properties of Al_2O_3–Na_2O–B_2O_3−Bi_2O_3 glasses using MCNPX Monte Carlo code *Mater. Chem. Phys.* **223** 209–19
[33] Gomaa H M, Sayyed M I, Tekin H O, Lakshminarayana G and EL-Dosokey A H 2019 Correlate the structural changes to gamma radiation shielding performance evaluation for some calcium bismuth-borate glasses containing *Nb2O5 Phys. B Condens. Matter* **567** 109–12
[34] Yu P, Zhang N Z, Cui Y T, Wu Z M, Wen L, Zeng Z Y and Xia L 2016 Achieving better magneto-caloric effect near room temperature in amorphous Gd50Co50 alloy by minor Zn addition *J. Non. Cryst. Solids* **434** 36–40
[35] Yuan F, Du J and Shen B 2012 Controllable spin-glass behavior and large magnetocaloric effect in Gd-Ni-Al bulk metallic glasses *Appl. Phys. Lett.* **101** 032405
[36] Li J, Xue L, Yang W, Yuan C, Huo J and Shen B 2018 Distinct spin glass behavior and excellent magnetocaloric effect in Er20Dy20Co20Al20RE20 (RE = Gd, Tb and Tm) high-entropy bulk metallic glasses *Intermetallics* **96** 90–3
[37] Xue L, Shao L, Luo Q and Shen B 2019 Gd25RE25Co25Al25 (RE = Tb, Dy and Ho) high-entropy glassy alloys with distinct spin-glass behavior and good magnetocaloric effect *J. Alloys Compd.* **790** 633–9
[38] Luo Q, Schwarz B, Mattern N and Eckert J 2012 Irreversible and reversible magnetic entropy change in a Dy-based bulk metallic glass *Intermetallics* **30** 76–9
[39] Huo J, Huo L, Men H, Wang X, Inoue A, Wang J, Chang C and Li R W 2015 The magnetocaloric effect of Gd-Tb-Dy-Al-M (M = Fe, Co and Ni) high-entropy bulk metallic glasses *Intermetallics* **58** 31–5
[40] Rammah Y S, Al-Buriahi M S and Abouhaswa A S 2020 B_2O_3–$BaCO_3$–Li_2O_3 glass system doped with Co_3O_4: Structure, optical, and radiation shielding properties *Phys. B Condens. Matter* **576** 411717
[41] Perişanoğlu U, El-Agawany F I, Kavaz E, Al-Buriahi M and Rammah Y S 2020 Surveying of Na2O3–BaO–PbO–Nb_2O_5–SiO_2–Al_2O_3 glass-ceramics system in terms of alpha, proton, neutron and gamma protection features by utilizing GEANT4 simulation codes *Ceram. Int.* **46** 3190–202
[42] Tonguc B T, Arslan H and Al-Buriahi M S 2018 Studies on mass attenuation coefficients, effective atomic numbers and electron densities for some biomolecules *Radiat. Phys. Chem.* **153** 86–91
[43] Al-Buriahi M S, Arslan H and Tonguc B T 2019 Investigation of photon energy absorption properties for some biomolecules *Nucl. Sci. Tech.* **30** 1–9
[44] Rammah Y S, Ali A A and El-Agawany F I 2019 γ-ray shielding features and crystallization of TiO2 borotellurite glasses *J. Non. Cryst. Solids* **526** 119720
[45] Rammah Y S, El-Agawany F I and El-Mesady I A 2019 Evaluation of photon attenuation and optical characterizations of bismuth lead borate glasses modified by TiO_2 *Appl. Phys. A Mater. Sci. Process.* **125** 727
[46] Al-Buriahi M S and Mann K S 2019 Radiation shielding investigations for selected tellurite-based glasses belonging to the TNW system *Mater. Res. Express* **6** 105206
[47] Al-Buriahi M S and Rammah Y S 2019 Electronic polarizability, dielectric, and gamma-ray shielding properties of some tellurite-based glasses *Appl. Phys. A Mater. Sci. Process.* **125** 678
[48] Al-Buriahi M S, Abouhaswa A S, Tekin H O, Sriwunkum C, El-Agawany F I, Nutaro T, Kavaz E and Rammah Y S 2020 Structure, optical, gamma-ray and neutron shielding properties of NiO doped B2O3–BaCO3–Li2O3 glass systems *Ceram. Int.* **46** 1711–21
[49] El-Agawany F I, Kavaz E, Perişanoğlu U, Al-Buriahi M and Rammah Y S 2019 Sm2O3 effects on mass stopping power/projected range and nuclear shielding characteristics of TeO_2–ZnO glass systems *Appl. Phys. A Mater. Sci. Process.* **125** 838
[50] Yildiz Yorgun N, Kavaz E, Tekin H O, Sayyed M I and Özdemir F 2019 Borax effect on gamma and neutron shielding features of lithium borate glasses: an experimental and monte carlo studies *Mater. Res. Express* **6** 115217
[51] Sayyed M I, Agar O, Kumar A, Tekin H O, Gaikwad D K and Obaid S S 2020 Shielding behaviour of (20 + x) Bi2O3—20BaO–10Na2O–10MgO–(40-x) B2O3: An experimental and Monte Carlo study *Chem. Phys.* **529** 110571
[52] Issa S A M, Ali A M, Tekin H O, Saddeek Y B, Al-Hajry A, Algarni H and Susoy G 2020 Enhancement of nuclear radiation shielding and mechanical properties of YBiBO3 glasses using La2O3 *Nucl. Eng. Technol.* **52** 1297–303
[53] Tekin H O and Kilicoglu O 2020 The influence of gallium (Ga) additive on nuclear radiation shielding effectiveness of Pd/Mn binary alloys *J. Alloys Compd.* **815** 152484
[54] Akman F, Sayyed M I, Kaçal M R and Tekin H O 2019 Investigation of photon shielding performances of some selected alloys by experimental data, theoretical and MCNPX code in the energy range of 81 keV–1333 keV *J. Alloys Compd.* **772** 516–24
[55] Agar O, Tekin H O, Sayyed M I, Korkmaz M E, Culfa O and Ertugay C 2019 Experimental investigation of photon attenuation behaviors for concretes including natural perlite mineral *Results Phys.* **12** 237–43
[56] Anon 2002 *RSICC Computer Code Collection, MCNPX User's Manual Version 2.4.0. Monte Carlo N-particle Transport Code System for Multiple and High Energy Applications*